

Nonequilibrium electron distribution function in a voltage-biased metal wire: A nonequilibrium Green's function approach

Taira Kawamura¹ and Yusuke Kato^{1,2}

¹*Department of Basic Science, The University of Tokyo, 3-8-1 Komaba, Tokyo 153-8902, Japan and*

²*Department of Physics, Graduate School of Science,*

The University of Tokyo, 7-3-1 Hongo, Tokyo 113-0033, Japan

(Dated: March 10, 2025)

We develop a theoretical framework to determine distribution functions in nonequilibrium systems coupled to equilibrium reservoirs, by using the nonequilibrium Green's function technique. As a paradigmatic example, we consider the nonequilibrium distribution function in a metal wire under a bias voltage. We model the system as a tight-binding chain connected to reservoirs with different electrochemical potentials at both ends. For electron scattering processes in the wire, we consider both elastic scattering from impurities and inelastic scattering from phonons within the self-consistent Born approximation. We demonstrate that the nonequilibrium distribution functions, as well as the electrostatic potential profiles, in various scattering regimes are well described within our framework. This scheme will contribute to advancing our understanding of quantum many-body phenomena driven by nonequilibrium distribution functions that have different functional forms from the equilibrium ones.

I. INTRODUCTION

Recent advances in experimental techniques for probing and controlling quantum many-body systems have stimulated theoretical interest in their nonequilibrium properties [1–27]. In particular, periodically driven Floquet systems [1–14] and open systems governed by non-Hermitian Hamiltonians [15–26] have attracted considerable attention due to their potential for realizing exotic quantum many-body states that have not been observed in thermal equilibrium systems. As exemplified by the Floquet/non-Hermitian topological band theories [7–14, 20–27], most theoretical studies of these systems have focused on nonequilibrium effects on their spectral properties, and the distribution functions describing their occupied states are assumed to follow the equilibrium forms, such as the Fermi-Dirac distribution function $f(\omega) = [1 + e^{(\omega - \mu_{\text{eff}})/T_{\text{eff}}}]^{-1}$ characterized by effective “temperature” T_{eff} and “chemical potential” μ_{eff} .

These effective parameters are physically meaningful quantities when systems are in local equilibrium, where the distribution function $f_x^{\text{neq}}(\omega)$ at each position x is well fitted by the equilibrium distribution functions [28, 29]. However, the fundamental differences in physical behavior between nonequilibrium quantum systems and their equilibrium counterparts emerge when the distribution function $f_x^{\text{neq}}(\omega)$ deviates significantly from the equilibrium forms. While effective temperature and chemical potential are ill-defined in such highly nonequilibrium states, the distribution function $f_x^{\text{neq}}(\omega)$ remains well-defined and serves as a useful quantity to characterize the nonequilibrium properties of systems. Thus, developing a theoretical framework to determine nonequilibrium distribution functions is crucial for exploring nonequilibrium quantum many-body phenomena beyond the local equilibrium paradigm.

A nonequilibrium system coupled to equilibrium reservoirs reaches a nonequilibrium steady state (NESS)

through the balance between driving forces and dissipations. The nonequilibrium distribution function in the NESS is determined by solving a boundary value problem, with the equilibrium distribution functions in the reservoirs serving as boundary conditions. A notable example of such nonequilibrium distribution functions is the “two-step distribution function” observed in mesoscopic systems under bias voltage [30–41]. In a metal wire between two reservoirs (electrodes) with different electrochemical potentials, electrons follow a position-dependent nonequilibrium distribution function $f_x^{\text{neq}}(\omega)$, as schematically illustrated in Fig. 1. This distribution function has been experimentally observed by superconducting tunneling spectroscopy [30–36], shot noise measurements [37], and using the Kondo effect in quantum dot systems [38]. In particular, when the wire length is shorter than the electron inelastic mean free path, a distribution function with a two-step structure emerges at low temperatures, reflecting the Fermi-Dirac distribution functions in the electrodes that have different electrochemical potentials (see Fig. 1). Similar two-step distribution functions have been observed in voltage-biased carbon nanotubes [39–41], and their potential realization in ultracold Fermi gases in a two-terminal configuration has also been explored [42, 43].

Nonequilibrium distribution functions such as the two-step distribution function can lead to a variety of interesting phenomena [44–62]. For instance, it has been experimentally demonstrated that the two-step distribution function can be used to control the critical current of a Josephson junction and realize π junction [44–49]. Moreover, the two-step distribution function can induce anomalous Fermi edge singularities [50] and spatially inhomogeneous Fulde-Ferrell-Larkin-Ovchinnikov-type superconducting states [51–54]. Besides these phenomena associated with the two-step distribution function, in two-dimensional electron gases in semiconductor heterostructures exposed to microwave radiation, oscilla-

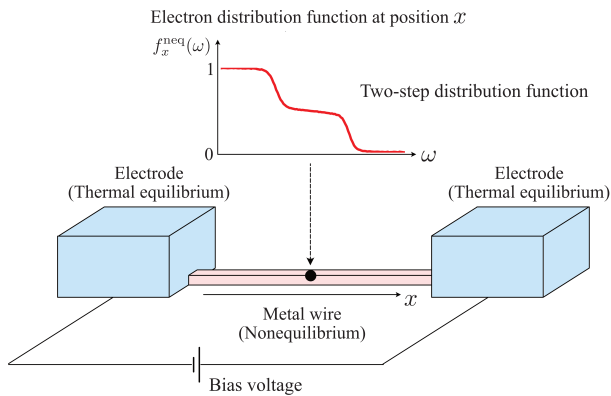


FIG. 1. A metal wire connected between two electrodes with different electrochemical potentials due to the bias voltage. These electrodes can be approximated as isolated systems in thermal equilibrium, where electrons follow the Fermi-Dirac distribution function. On the other hand, electrons at position x in the wire follow a nonequilibrium distribution function $f_x^{\text{neq}}(\omega)$, which in general has a different functional form from the Fermi-Dirac distribution function. The form of the nonequilibrium distribution function $f_x^{\text{neq}}(\omega)$ depends on scattering processes experienced by electrons as they traverse the wire [30–40]. When the wire length is shorter than the electron inelastic mean free path, $f_x^{\text{neq}}(\omega)$ exhibits the two-step structure at low temperatures, reflecting the different electrochemical potentials in the electrodes.

tory structure in the distribution function is known to induce magnetoresistance oscillations [55–58]. In superconductors under quasiparticle injection, the nonequilibrium quasiparticle distribution generates the pair-quasiparticle potential difference, known as charge imbalance [59–62]. The proper description of nonequilibrium distribution functions is crucial for understanding these nonequilibrium phenomena beyond the local equilibrium paradigm.

In this paper, we develop a theoretical framework to determine position-dependent distribution functions $f_x^{\text{neq}}(\omega)$ in nonequilibrium systems coupled to equilibrium reservoirs, by employing the nonequilibrium Green’s function technique [63–65]. While the nonequilibrium Green’s function technique has been widely used to study nonequilibrium quantum systems [63–65], its application to the boundary value problems for nonequilibrium distribution functions is very limited. As a paradigmatic example, we consider a nonequilibrium distribution function $f_x^{\text{neq}}(\omega)$ in a voltage-biased metal wire illustrated in Fig. 1. In this system, the electrodes connected to both ends of the wire can be approximated as reservoirs in thermal equilibrium, which serve as the boundary conditions for the nonequilibrium distribution function in the wire. The form of the distribution function $f_x^{\text{neq}}(\omega)$ depends on scattering processes experienced by electrons as they traverse the wire [30–40]. We consider elastic scattering from impurities, as well as inelastic scattering from phonons, and systematically investigate how these scattering processes affect the form of the distribution function $f_x^{\text{neq}}(\omega)$.

We make a remark on the difference between the nonequilibrium Green’s function approach and the transport equation approach used in previous work [66–69]. The nonequilibrium (Wigner) distribution function $f_x^{\text{neq}}(\mathbf{p})$ follows the Boltzmann equation [70]

$$[v_x \partial_x + e\mathbf{E} \cdot \partial_{\mathbf{p}}] f_x^{\text{neq}}(\mathbf{p}) = I_{\text{coll}} \{ f_x^{\text{neq}}(\mathbf{p}) \}, \quad (1)$$

which describes the semiclassical motion of an electron with momentum $\mathbf{p} = m\mathbf{v}$ in the electric field \mathbf{E} . Here, we use the one-dimensional form, assuming homogeneity in the other two directions. In Eq. (1), I_{coll} is the collision term, which describes the electron scattering effects. In the case of strong impurity scattering (diffusive limit), the distribution function is almost isotropic in momentum \mathbf{p} space, and it can be regarded as a function of the electron kinetic energy $\omega = \mathbf{p}^2/(2m)$. Averaging over momentum directions in Eq. (1), one obtains the equation for the distribution function as [66–70]

$$D \partial_x^2 f_x^{\text{neq}}(\omega) = I_{\text{inel}} \{ f_x^{\text{neq}}(\omega) \}, \quad (2)$$

where D is the diffusion constant and I_{inel} describes the effects of inelastic electron scattering. In previous work [66–69], the nonequilibrium distribution function in the metal wire depicted in Fig. 1 is determined by solving Eq. (2) with boundary conditions

$$f_{x=0}(\omega) = f(\omega - \mu_L), \quad (3)$$

$$f_{x=L}(\omega) = f(\omega - \mu_R), \quad (4)$$

which are imposed by the reservoirs at both ends of the wire. Here, L denotes the wire length and $f(\omega - \mu_{\alpha=L,R})$ is the Fermi-Dirac distribution function in the left and right reservoir with the electrochemical potential μ_{α} . This approach, however, has a limitation. Since Eq. (2) is applicable only in the diffusive limit, we need to solve the more general Boltzmann equation (1) to deal with systems in the ballistic-diffusive crossover regime. However, we cannot impose the two boundary conditions, such as Eqs. (3) and (4), on the Boltzmann equation (1) because it is a first-order differential equation with respect to x . Thus, the applicability of the transport equation approach to boundary value problems for nonequilibrium distribution functions is restricted to systems in the diffusive limit. In contrast, the nonequilibrium Green’s function approach, which incorporates system-reservoir coupling effects through self-energy corrections, does not suffer from the difficulty of imposing boundary conditions. As a result, this approach enables a unified description of nonequilibrium distribution functions across the ballistic-diffusive crossover regime.

This paper is organized as follows. In Sec. II, we present our model of a voltage-biased metal wire and explain how to determine the nonequilibrium distribution function in the wire by using the nonequilibrium Green’s function technique. In Sec. III, we show the calculated nonequilibrium distribution function and discuss electron scattering effects. Throughout this paper, we set $\hbar = k_B = 1$ and take $e < 0$.

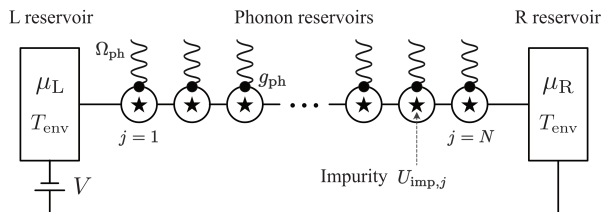


FIG. 2. Schematic picture of our model. Two free-fermion α ($= L, R$) reservoirs are connected to both ends of the tight-binding chain with N sites. The α reservoir is in the thermal equilibrium state characterized by the electrochemical potential μ_α and the temperature T_{env} . The potential difference $\mu_L - \mu_R$ equals the applied bias voltage eV across the wire. Within the chain, electrons scatter from randomly distributed impurities with the potential $U_{\text{imp},j}$. The electrons also interact with local phonons of frequency Ω_{ph} , where g_{ph} represents the electron-phonon coupling constant.

II. FORMALISM

A. Model

We consider a metal wire connected between two electrodes with different electrochemical potentials. For simplicity, we assume that the wire is quasi-one-dimensional and no changes take place in y and z directions. The system, depicted in Fig. 2, is described by the Hamiltonian

$$H = H_0 + H_{\text{lead}} + H_t + H_{\text{imp}} + H_{\text{ph}} + H_{\text{e-ph}}, \quad (5)$$

where

$$H_0 = -t \sum_{j=1}^{N-1} [c_j^\dagger c_{j+1} + \text{H.c.}] + e \sum_{j=1}^N \varphi_j c_j^\dagger c_j \quad (6)$$

describes the quasi-one-dimensional metal wire. Here, N denotes the number of lattice sites, $-t$ is the nearest-neighbor hopping amplitude, and φ_j represents the electrostatic potential at site j ($= 1, \dots, N$). For simplicity, we neglect spin-dependent interactions in this work, which allows us to treat the electrons as spinless. For later convenience, we define a parameter

$$x_j = \frac{j-1}{N-1}, \quad (7)$$

which specifies the distance from the left end of the wire.

The electrodes connected to both ends of the wire are described by H_{lead} , having the form

$$H_{\text{lead}} = \sum_{\alpha=L,R} \sum_{\mathbf{k}} \xi_{\alpha,\mathbf{k}} a_{\alpha,\mathbf{k}}^\dagger a_{\alpha,\mathbf{k}}. \quad (8)$$

Here, $a_{\alpha,\mathbf{k}}^\dagger$ creates an electron with kinetic energy $\xi_{\alpha,\mathbf{k}}$ in the α ($=L, R$) reservoir. The reservoirs are assumed to be in the thermal equilibrium state characterized by their electrochemical potential μ_α and temperature T_{env} .

Under this assumption, electrons in the α reservoir follow the Fermi-Dirac distribution function,

$$f(\omega - \mu_\alpha) = \frac{1}{e^{(\omega - \mu_\alpha)/T_{\text{env}}} + 1}. \quad (9)$$

The applied bias voltage eV across the wire equals the electrochemical potential difference $\mu_L - \mu_R$ between the left and right reservoirs.

The coupling between the wire and the electrodes is described by

$$H_t = - \sum_{\mathbf{k}} [t_L a_{L,\mathbf{k}}^\dagger c_1 + \text{H.c.}] - \sum_{\mathbf{k}} [t_R a_{R,\mathbf{k}}^\dagger c_N + \text{H.c.}]. \quad (10)$$

Here, $-t_\alpha$ is the hopping amplitude between the wire and the α reservoir. For simplicity, we consider the case of symmetric coupling ($t_L = t_R \equiv t_{\text{lead}}$), which allows us to set $\mu_L = +eV/2$ (> 0) and $\mu_R = -eV/2$.

The form of the electron distribution function reflects the scattering processes experienced by electrons as they traverse the wire. In this work, we examine how the distribution function is affected by two scattering processes: *elastic* scattering from (non-magnetic) impurities and *inelastic* scattering from phonons. The elastic scattering is described by H_{imp} in Eq. (5), having the form

$$H_{\text{imp}} = \sum_{j=1}^N U_{\text{imp},j} c_j^\dagger c_j. \quad (11)$$

Here, $U_{\text{imp},j}$ represents the impurity scattering potential at site j , given by

$$U_{\text{imp},j} = u_{\text{imp}} \sum_{k=1}^{N_{\text{imp}}} \delta_{j,k}, \quad (12)$$

with N_{imp} being the number of impurities in the wire.

The phonons are introduced as local harmonic oscillators at each site, known as the Holstein model in the literature [64, 71, 72]. The phonon reservoirs are described by

$$H_{\text{ph}} = \sum_{j=1}^N \Omega_0 b_j^\dagger b_j, \quad (13)$$

where Ω_0 represents the phonon frequency and b_j denotes the phonon annihilation operator at site j . The electron-phonon interaction in the wire is described by

$$H_{\text{e-ph}} = g_{\text{ph}} \sum_{j=1}^N a_j^\dagger a_j [b_j + b_j^\dagger], \quad (14)$$

where g_{ph} represents the electron-phonon coupling constant. In this model, the strength of the electron-phonon coupling can be characterized by the parameter

$$\gamma_{\text{ph}} \equiv 2g_{\text{ph}}^2/\Omega_0, \quad (15)$$

which gives the strength of the phonon-mediated on-site attractive interaction in the antiadiabatic limit.

We note that electron-electron scattering also affects the form of the distribution function [30–36, 70]. It is known that in mesoscale ($\sim 1\mu\text{m}$) diffusive metal wires, electron-electron scattering due to screened Coulomb interactions dominates over electron-phonon scattering at low temperatures, typically below 1K [70, 73–75]. Moreover, a tiny concentration of magnetic impurities with a small Kondo temperature enhances electron-electron scattering effects [32–36, 75–77]. However, the theoretical treatment of these strong correlation effects is beyond the scope of this study.

B. Nonequilibrium Green's function

To determine the nonequilibrium distribution function in the metal wire, we conveniently introduce a $N \times N$ matrix nonequilibrium Green's function, given by

$$\mathbf{G}^{\mathcal{X}=\mathcal{R},\mathcal{A},\lessgtr}(t, t') = \begin{pmatrix} G_{11}^{\mathcal{X}}(t, t') & \cdots & G_{1N}^{\mathcal{X}}(t, t') \\ \vdots & \ddots & \vdots \\ G_{N1}^{\mathcal{X}}(t, t') & \cdots & G_{NN}^{\mathcal{X}}(t, t') \end{pmatrix}, \quad (16)$$

where

$$\begin{aligned} G_{jk}^{\mathcal{R}}(t, t') &= -i\Theta(t - t') \langle [c_j(t), c_k^\dagger(t')]_+ \rangle \\ &= [G_{kj}^{\mathcal{A}}(t', t)]^*, \end{aligned} \quad (17a)$$

$$G_{jk}^{\lessgtr}(t, t') = i \langle c_k^\dagger(t') c_j(t) \rangle, \quad (17b)$$

$$G_{jk}^{\gtr}(t, t') = -i \langle c_j(t) c_k^\dagger(t') \rangle, \quad (17c)$$

with $[A, B]_\pm = AB \pm BA$. In Eq. (16), $\mathbf{G}^{\mathcal{R}}$, $\mathbf{G}^{\mathcal{A}}$, \mathbf{G}^{\lessgtr} , and \mathbf{G}^{\gtr} are, respectively, the retarded, advanced, lesser, and greater Green's functions.

When the system is in a NESS, these nonequilibrium Green's functions satisfy the Dyson equations [63–65],

$$\mathbf{G}^{\mathcal{R}(\mathcal{A})}(\omega) = \mathbf{G}_0^{\mathcal{R}(\mathcal{A})}(\omega) + \mathbf{G}_0^{\mathcal{R}(\mathcal{A})}(\omega) \boldsymbol{\Sigma}^{\mathcal{R}(\mathcal{A})}(\omega) \mathbf{G}^{\mathcal{R}(\mathcal{A})}(\omega), \quad (18)$$

$$\mathbf{G}^{\lessgtr}(\omega) = \mathbf{G}^{\mathcal{R}}(\omega) \boldsymbol{\Sigma}^{\lessgtr}(\omega) \mathbf{G}^{\mathcal{A}}(\omega). \quad (19)$$

Here, $\mathbf{G}_0^{\mathcal{R}(\mathcal{A})}$ denotes the bare Green's function of the *isolated* metal wire without electron scattering, given by

$$\mathbf{G}_0^{\mathcal{R}(\mathcal{A})}(\omega) = \frac{1}{\omega \pm i\delta - \mathcal{H}_0}, \quad (20)$$

where δ represents an infinitesimally small positive number and \mathcal{H}_0 is the matrix representation of the Hamiltonian H_0 in Eq. (6). In Eqs. (18) and (19), $\boldsymbol{\Sigma}^{\mathcal{X}}$ is the $N \times N$ matrix self-energy correction, which consists of three parts,

$$\boldsymbol{\Sigma}^{\mathcal{X}}(\omega) = \boldsymbol{\Sigma}_{\text{lead}}^{\mathcal{X}}(\omega) + \boldsymbol{\Sigma}_{\text{imp}}^{\mathcal{X}}(\omega) + \boldsymbol{\Sigma}_{\text{ph}}^{\mathcal{X}}(\omega). \quad (21)$$

Here, $\boldsymbol{\Sigma}_{\text{lead}}^{\mathcal{X}}$, $\boldsymbol{\Sigma}_{\text{imp}}^{\mathcal{X}}$, and $\boldsymbol{\Sigma}_{\text{ph}}^{\mathcal{X}}$ describe the effects of reservoir couplings, elastic scattering from impurities, and inelastic scattering from phonons, respectively.

In the second-order Born approximation with respect to the tunneling amplitude $t_\alpha = t_{\text{lead}}$, $\boldsymbol{\Sigma}_{\text{lead}}^{\mathcal{X}}$ describing the couplings with the reservoirs takes the form [64, 65]

$$\Sigma_{\text{lead},jk}^{\mathcal{X}}(\omega) = |t_{\text{lead}}|^2 \sum_{\mathbf{k}} [\mathcal{G}_{\text{L},\mathbf{k}}^{\mathcal{X}}(\omega) \delta_{j,1} + \mathcal{G}_{\text{R},\mathbf{k}}^{\mathcal{X}}(\omega) \delta_{j,N}] \delta_{j,k}. \quad (22)$$

Here, the noninteracting Green's functions in the α ($=$ L, R) reservoir are given by [63–65]

$$\mathcal{G}_{\alpha,\mathbf{k}}^{\mathcal{R}(\mathcal{A})}(\omega) = \frac{1}{\omega \pm i\delta - \xi_{\alpha,\mathbf{k}}}, \quad (23a)$$

$$\mathcal{G}_{\alpha,\mathbf{k}}^{\lessgtr}(\omega) = 2\pi i \delta(\omega - \xi_{\alpha,\mathbf{k}}) f(\omega - \mu_\alpha), \quad (23b)$$

$$\mathcal{G}_{\alpha,\mathbf{k}}^{\gtr}(\omega) = -2\pi i \delta(\omega - \xi_{\alpha,\mathbf{k}}) f(-\omega + \mu_\alpha). \quad (23c)$$

Under the wide-band limit approximation [64, 65], which assumes a constant density of states $\nu_\alpha(\omega) \equiv \nu$ in the reservoirs around the Fermi level $\omega = 0$, the \mathbf{k} summation in Eq. (22) yields

$$\boldsymbol{\Sigma}_{\alpha,\text{lead}}^{\mathcal{R}(\mathcal{A})}(\omega) = \mp i \boldsymbol{\Gamma}_\alpha, \quad (24a)$$

$$\boldsymbol{\Sigma}_{\alpha,\text{lead}}^{\lessgtr}(\omega) = 2i \boldsymbol{\Gamma}_\alpha f(\omega - \mu_\alpha), \quad (24b)$$

$$\boldsymbol{\Sigma}_{\alpha,\text{lead}}^{\gtr}(\omega) = -2i \boldsymbol{\Gamma}_\alpha f(-\omega + \mu_\alpha), \quad (24c)$$

with

$$\boldsymbol{\Sigma}_{\text{lead}}^{\mathcal{X}}(\omega) = \sum_{\alpha=\text{L,R}} \boldsymbol{\Sigma}_{\alpha,\text{lead}}^{\mathcal{X}}(\omega), \quad (25)$$

$$[\boldsymbol{\Gamma}_{\text{L}}]_{ij} = \gamma_{\text{lead}} \delta_{i,j} \delta_{i,1}, \quad (26)$$

$$[\boldsymbol{\Gamma}_{\text{R}}]_{ij} = \gamma_{\text{lead}} \delta_{i,j} \delta_{i,N}, \quad (27)$$

$$\gamma_{\text{lead}} = \pi \nu |t_{\text{lead}}|^2. \quad (28)$$

This wide-band limit approximation is valid when the energy dependence of the density of states $\nu_\alpha(\omega)$ in the reservoirs can be ignored around the Fermi level $\omega = 0$, within the range of applied bias voltage eV [51].

We deal with the self-energy correction $\boldsymbol{\Sigma}_{\text{imp}}^{\mathcal{X}}$ describing electron-impurity scattering effects within the self-consistent Born approximation [63, 65], which yields

$$\Sigma_{\text{imp},jk}^{\mathcal{X}}(\omega) = U_{\text{imp},j} U_{\text{imp},k} G_{jk}^{\mathcal{X}}(\omega). \quad (29)$$

After spatial averaging over impurity positions, we obtain [78]

$$\begin{aligned} \boldsymbol{\Sigma}_{\text{imp}}^{\mathcal{X}}(\omega) &= \gamma_{\text{imp}}^2 \begin{pmatrix} G_{11}^{\mathcal{X}}(\omega) & & 0 \\ & \ddots & \\ 0 & & G_{NN}^{\mathcal{X}}(\omega) \end{pmatrix} \\ &= \gamma_{\text{imp}}^2 \mathbf{1} \otimes \mathbf{G}^{\mathcal{X}}(\omega). \end{aligned} \quad (30)$$

Here, $\mathbf{1}$ denotes the $N \times N$ unit matrix and \otimes represents the Kronecker product. The parameter

$$\gamma_{\text{imp}}^2 = N_{\text{imp}} u_{\text{imp}}^2 / N \quad (31)$$

characterizes the impurity scattering strength: $\gamma_{\text{imp}} = 0$ (large γ_{imp}) corresponds to the ballistic (diffusive) limit.

We note that in the presence of strong impurity scattering, the system is characterized by a rapidly varying potential, leading to electron localization within potential wells (Anderson localization) [70, 79]. However, this localized regime lies beyond the scope of this paper.

Within the self-consistent Born approximation [63, 65], the self-energy $\Sigma_{\text{ph}}^{\text{X}}$ describing electron-phonon scattering effects takes the form

$$\begin{aligned} \Sigma_{\text{ph}}^{\mathcal{R}(\mathcal{A})}(\omega) &= ig_{\text{ph}}^2 \int_{-\infty}^{\infty} \frac{d\nu}{2\pi} \left[D^{\mathcal{R}(\mathcal{A})}(\nu) \mathbf{1} \otimes \mathbf{G}^<(\omega - \nu) \right. \\ &\quad + D^{\mathcal{R}(\mathcal{A})}(\nu) \mathbf{1} \otimes \mathbf{G}^{\mathcal{R}(\mathcal{A})}(\omega - \nu) \\ &\quad \left. + D^<(\nu) \mathbf{1} \otimes \mathbf{G}^{\mathcal{R}(\mathcal{A})}(\omega - \nu) \right], \end{aligned} \quad (32a)$$

$$\Sigma_{\text{ph}}^{\leq}(\omega) = ig_{\text{ph}}^2 \int_{-\infty}^{\infty} \frac{d\nu}{2\pi} D^{\leq}(\nu) \mathbf{1} \otimes \mathbf{G}^{\leq}(\omega - \nu). \quad (32b)$$

Here, D^{X} is the phonon Green's function, which is given by [63, 65]

$$D^{\mathcal{R}(\mathcal{A})}(\nu) = \frac{1}{\nu - \Omega_0 \pm i\delta} + \frac{1}{\nu + \Omega_0 \pm i\delta}, \quad (33a)$$

$$D^{\leq}(\nu) = -2\pi i [\delta(\nu - \Omega_0) + \delta(\nu + \Omega_0)] n_{\text{B}}(\pm\nu), \quad (33b)$$

with the Bose-Einstein distribution function,

$$n_{\text{B}}(\nu) = \frac{1}{e^{\nu/T_{\text{env}}} - 1}. \quad (34)$$

In deriving $\Sigma_{\text{ph}}^{\text{X}}$, we have assumed that phonons are unperturbed by electron-phonon couplings and maintain thermal equilibrium at temperature T_{env} [80]. Substituting Eq. (33b) into Eq. (32b) yields

$$\begin{aligned} \Sigma_{\text{ph}}^{\leq}(\omega) &= g_{\text{ph}}^2 \left[[n_{\text{B}}(\Omega_0) + 1] \mathbf{1} \otimes \mathbf{G}^{\leq}(\omega \pm \Omega_0) \right. \\ &\quad \left. + n_{\text{B}}(\Omega_0) \mathbf{1} \otimes \mathbf{G}^{\leq}(\omega \mp \Omega_0) \right]. \end{aligned} \quad (35)$$

We note that unlike the lesser and greater components $\Sigma_{\text{ph}}^{\leq}$, the ν integral in Eq. (32a) cannot be performed analytically. The efficient numerical computation of the retarded component $\Sigma_{\text{ph}}^{\mathcal{R}}$ is detailed in Appendix A 1.

The dressed Green's functions are obtained by incorporating all self-energy corrections into the Dyson equations (18) and (19). From Eq. (18), the retarded Green's function is obtained as

$$\begin{aligned} \mathbf{G}^{\mathcal{R}}(\omega) &= \frac{1}{\omega - \mathcal{H}_0 - \Sigma_{\text{lead}}^{\mathcal{R}}(\omega) - \Sigma_{\text{imp}}^{\mathcal{R}}(\omega) - \Sigma_{\text{ph}}^{\mathcal{R}}(\omega)} \\ &\equiv \mathbf{T}^{-1}. \end{aligned} \quad (36)$$

The tridiagonal structure of \mathbf{T} allows for efficient and stable computation of \mathbf{T}^{-1} . The numerical implementation is presented in Appendix A 2.

The lesser Green's function $\mathbf{G}^<$ is obtained by substituting the dressed retarded Green's function in Eq. (36) into the Dyson equation (19). Noting that $\Sigma^< = \Sigma_{\text{lead}}^< +$

$\Sigma_{\text{imp}}^< + \Sigma_{\text{ph}}^<$ is a diagonal matrix, we have

$$\begin{aligned} G_{jj}^<(\omega) &= \sum_{l,m=1}^N G_{jl}^{\mathcal{R}}(\omega) \Sigma_{lm}^<(\omega) G_{mk}^{\mathcal{A}}(\omega) \\ &= \sum_{l=1}^N |G_{jl}^{\mathcal{R}}(\omega)|^2 \Sigma_{ll}^<(\omega). \end{aligned} \quad (37)$$

Since the self-energy corrections $\Sigma_{\text{imp}}^{\text{X}}$ and $\Sigma_{\text{ph}}^{\text{X}}$ involve the dressed Green's function \mathbf{G}^{X} , a self-consistent calculation is required. To accelerate the convergence of this self-consistent loop, we employ the restarted Pulay mixing scheme [81–83].

Once we obtain the dressed Green's functions, the local density of states $\nu_j(\omega)$, the filling fraction n_j , and the nonequilibrium distribution function $f_j^{\text{neq}}(\omega)$ at site j are, respectively, obtained as [63–65, 84, 85]

$$\nu_j(\omega) = -\frac{1}{\pi} \text{Im} G_{jj}^{\mathcal{R}}(\omega), \quad (38)$$

$$n_j = -i \int_{-\infty}^{\infty} \frac{d\omega}{2\pi} G_{jj}^<(\omega), \quad (39)$$

$$f_j^{\text{neq}}(\omega) = \frac{-i G_{jj}^<(\omega)}{2\pi \nu_j(\omega)}. \quad (40)$$

We note that the charge current through the wire can also be evaluated using the dressed Green's function \mathbf{G}^{X} , as detailed in Appendix B.

The requirement of charge neutrality in the metal wire imposes the condition [70]

$$\Delta n_j = n_j - n_j^0 = 0, \quad (j = 1, \dots, N) \quad (41)$$

where n_j^0 represents the filling fraction in the absence of bias voltage V (that is, $\mu_{\text{L}} = \mu_{\text{R}}$). The electrostatic potential φ_j is determined by solving the simultaneous nonlinear equations (41) with the Broyden method [86, 87].

III. NONEQUILIBRIUM DISTRIBUTION FUNCTION IN A VOLTAGE-BIASED METAL WIRE

Figure 3 shows the calculated electron distribution function $f_j^{\text{neq}}(\omega)$ in a metal wire under bias voltage. In this figure, we set $eV/t = 0.4$, corresponding to the linear transport regime (see Appendix B). In the following, we discuss the effects of elastic and inelastic electron scattering on the distribution function in turn.

A. Crossover from the ballistic to the diffusive regime

We first discuss the changes in the form of the distribution function $f_j^{\text{neq}}(\omega)$ due to elastic scattering from

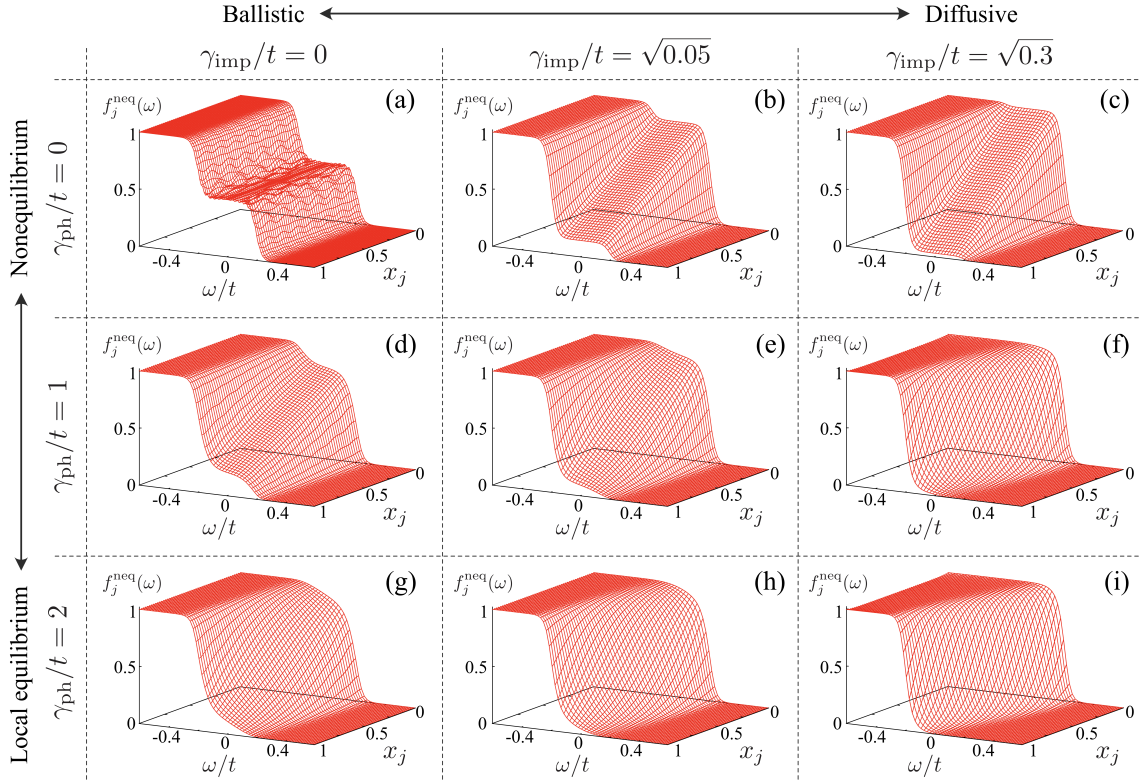


FIG. 3. Calculated electron distribution function $f_j^{\text{neq}}(\omega)$ in a metal wire under bias voltage. The position x_j along the wire is defined by Eq. (7). We show results for different values of impurity scattering strength γ_{imp} and electron-phonon coupling strength γ_{ph} . We set $N = 201$, $eV/t = 0.4$, $\gamma_{\text{lead}}/t = 1$, and $T_{\text{env}}/t = 0.02$. These values are also used in the following figures.

impurities, shown in Fig. 3(a)-(c). In the ballistic limit ($\gamma_{\text{ph}} = \gamma_{\text{imp}} = 0$), where electrons traverse the metal wire without any scattering, the local density of states $\nu_j(\omega)$ in Eq. (38) can be expressed as

$$\begin{aligned} \nu_j(\omega) &= \frac{i}{2\pi} [G_{jj}^{\mathcal{R}}(\omega) - G_{jj}^{\mathcal{A}}(\omega)] \\ &= \frac{i}{2\pi} \sum_{l,m=1}^N G_{jl}^{\mathcal{R}}(\omega) [\Sigma_{\text{lead},lm}^{\mathcal{R}} - \Sigma_{\text{lead},lm}^{\mathcal{A}}](\omega) G_{mj}^{\mathcal{A}}(\omega) \\ &= \frac{\gamma_{\text{lead}}}{\pi} [|G_{j1}^{\mathcal{R}}(\omega)|^2 + |G_{jN}^{\mathcal{R}}(\omega)|^2]. \end{aligned} \quad (42)$$

Here, we have used [65]

$$\begin{aligned} G_{jk}^{\mathcal{R}}(\omega) &= [G_{kj}^{\mathcal{A}}(\omega)]^*, \\ G_{jj}^{\mathcal{R}}(\omega) - G_{jj}^{\mathcal{A}}(\omega) &= \sum_{l,m=1}^N G_{jl}^{\mathcal{R}}(\omega) [\Sigma_{lm}^{\mathcal{R}} - \Sigma_{lm}^{\mathcal{A}}](\omega) G_{mj}^{\mathcal{A}}(\omega). \end{aligned} \quad (44)$$

In the ballistic limit, the lesser Green's function $G_{jj}^<(\omega)$ in Eq. (37) is reduced to

$$\begin{aligned} G_{jj}^<(\omega) &= 2i\gamma_{\text{lead}} \left[f(\omega - \mu_{\text{L}}) |G_{j1}^{\mathcal{R}}(\omega)|^2 \right. \\ &\quad \left. + f(\omega - \mu_{\text{R}}) |G_{jN}^{\mathcal{R}}(\omega)|^2 \right]. \end{aligned} \quad (45)$$

Using Eqs. (40), (42) and (45), we obtain the nonequilibrium distribution function $f_j^{\text{neq}}(\omega)$ in the ballistic limit as

$$f_j^{\text{neq}}(\omega) = w_j(\omega) f(\omega - \mu_{\text{L}}) + [1 - w_j(\omega)] f(\omega - \mu_{\text{R}}), \quad (46)$$

where we define the weight function as

$$w_j(\omega) = \frac{|G_{j1}^{\mathcal{R}}(\omega)|^2}{|G_{j1}^{\mathcal{R}}(\omega)|^2 + |G_{jN}^{\mathcal{R}}(\omega)|^2}. \quad (47)$$

Equation (46) clearly shows that the distribution function $f_j^{\text{neq}}(\omega)$, which describes the probability of observing an electron with energy ω at site j , is given by the sum of the two probabilities: (1) $w_j(\omega) f(\omega - \mu_{\text{L}})$, the probability of an electron with energy ω propagating from the left reservoir, and (2) $[1 - w_j(\omega)] f(\omega - \mu_{\text{R}})$, the probability of an electron propagating from the right reservoir.

In the ballistic limit, the amplitude $|G_{j1}^{\mathcal{R}}(\omega)|^2$, which represents the propagation probability of electron with energy ω from site 1 to j , should be independent of the site index j due to the absence of scattering. Therefore, we expect $|G_{j1}^{\mathcal{R}}(\omega)|^2 \simeq |G_{jN}^{\mathcal{R}}(\omega)|^2 (\simeq |G_{N1}^{\mathcal{R}}(\omega)|^2)$, leading to $w_j(\omega) \simeq 0.5$. This is verified in Fig. 4(a), which shows that $w_j(\omega)$ is constant over space, except for the minor oscillations around $w_j(\omega) = 0.5$. Using this fact, one can approximate Eq. (46) as

$$f_j^{\text{neq}}(\omega) \simeq \frac{1}{2} [f(\omega - \mu_{\text{L}}) + f(\omega - \mu_{\text{R}})]. \quad (48)$$

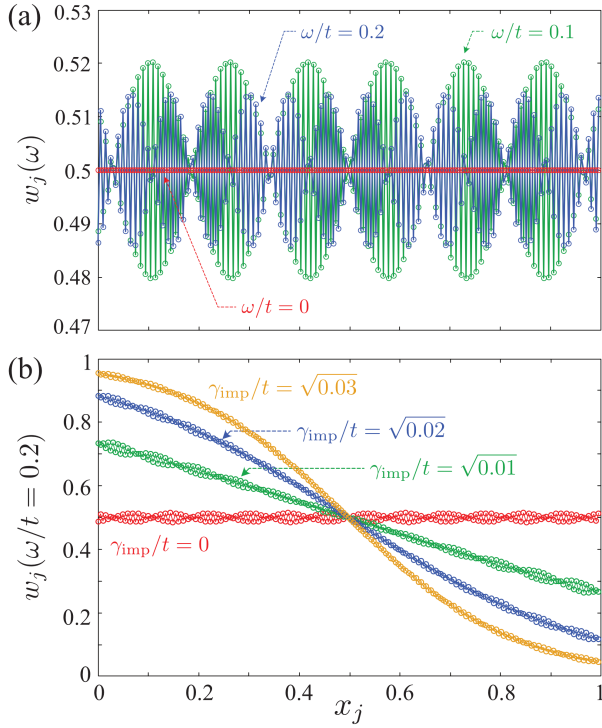


FIG. 4. (a) Position x_j dependence of the weight function $w_j(\omega)$ in Eq. (47). We show the results for $\omega/t = 0, 0.1$, and 0.2 . (b) Impurity scattering strength γ_{imp} dependence of the weight function $w_j(\omega)$. As a typical example, we take $\omega/t = 0.2$.

Thus, in the ballistic limit, the distribution function $f_j^{\text{neq}}(\omega)$ is simply expressed as the average of the Fermi-Dirac distribution functions in the left and right reservoirs, and does not depend on the position x_j along the wire [31, 34–36, 70], as shown in Fig. 3(a). We also see from Eq. (48) that the distribution function $f_j^{\text{neq}}(\omega)$ exhibits the two-step structure at low temperatures ($T_{\text{env}} \ll \mu_L - \mu_R$), reflecting the different Fermi-Dirac distribution function $f(\omega - \mu_\alpha)$ in the α reservoir.

We briefly note that the spatial oscillations in the weight function $w_j(\omega)$ arise from Fabry-Perot-like interference between the left and right reservoirs, which act as potential barriers [88, 89]. These oscillations in the weight function $w_j(\omega)$ result in the oscillations in the distribution function $f_j^{\text{neq}}(\omega)$ around $|\omega| \lesssim [\mu_L - \mu_R]/2 = 0.2t$, as shown in Fig. 3(a).

Figures 3(b) and (c) show that elastic scattering from impurities results in a spatially varying distribution function $f_j^{\text{neq}}(\omega)$. Figure 5 shows the distribution function at three positions: $x_j = 0.1$ (near the left reservoir), $x_j = 0.5$ (in the middle of the wire), and $x_j = 0.9$ (near the right reservoir), for different impurity scattering strengths γ_{imp} . In the presence of electron-impurity scattering, electrons traverse the wire via a random walk process. As a result, the distribution function at site j more strongly reflects the Fermi-Dirac distribution func-

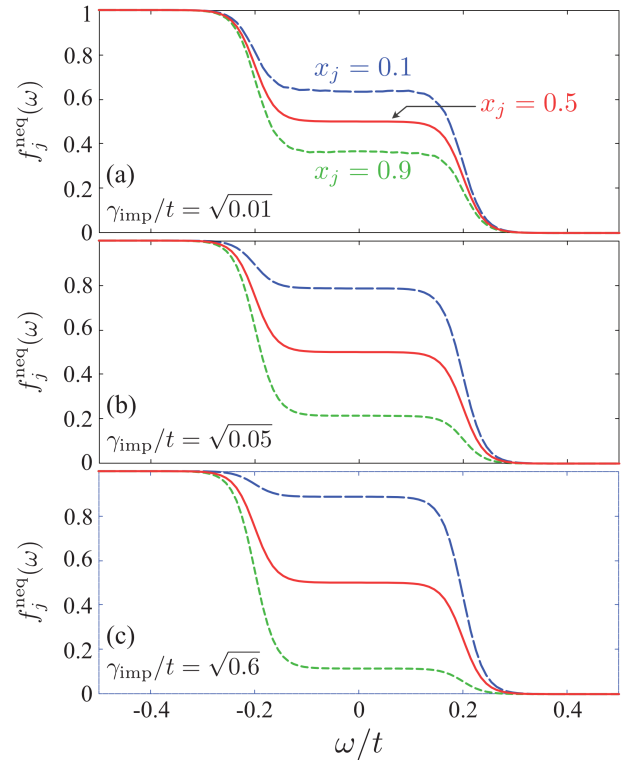


FIG. 5. Calculated distribution function $f_j^{\text{neq}}(\omega)$ for (a) $\gamma_{\text{imp}}/t = \sqrt{0.01}$, (b) $\gamma_{\text{imp}}/t = \sqrt{0.05}$, and (c) $\gamma_{\text{imp}}/t = \sqrt{0.6}$. We show the distribution function at $x_j = 0.1$ (near the left reservoir), $x_j = 0.5$ (in the middle of the wire), and $x_j = 0.9$ (near the right reservoir). We set $\gamma_{\text{ph}} = 0$ for all panels.

tion in the reservoir closer to site j .

Although the distribution function $f_j^{\text{neq}}(\omega)$ deviates from Eq. (46) in the presence of impurity scattering, its overall behavior can be reasonably described by Eq. (46), as demonstrated in Fig. 6. This allows us to analyze the spatial dependence of the distribution function $f_j^{\text{neq}}(\omega)$ in the ballistic-diffusive crossover regime using the weight function $w_j(\omega)$ in Eq. (47). Figure 4(b) shows that in the presence of impurity scattering ($\gamma_{\text{imp}} \neq 0$), the weight function $w_j(\omega)$ decreases with increasing x_j . Since the weight function $w_j(\omega)$ physically represents the probability of an electron with energy ω propagating from the left reservoir to site j , Fig. 4 (b) indicates that information about the distribution function $f(\omega - \mu_\alpha)$ in the α reservoir is gradually lost due to elastic scattering from impurities as electrons propagate away from the α reservoir. We note that impurity scattering suppresses Fabry-Perot-like interference between the reservoirs [89], which reduces oscillations in the weight function $w_j(\omega)$, as shown in Fig. 4 (b). As a result, the oscillations in $f_j^{\text{neq}}(\omega)$ around $|\omega| \lesssim [\mu_L - \mu_R]/2$ are also suppressed with increasing γ_{imp} , as shown in Fig. 3 (a)-(c).

We see from Fig. 3(c) that in the diffusive (large γ_{imp}) limit, the distribution function linearly interpolates between the Fermi-Dirac distribution functions in the left

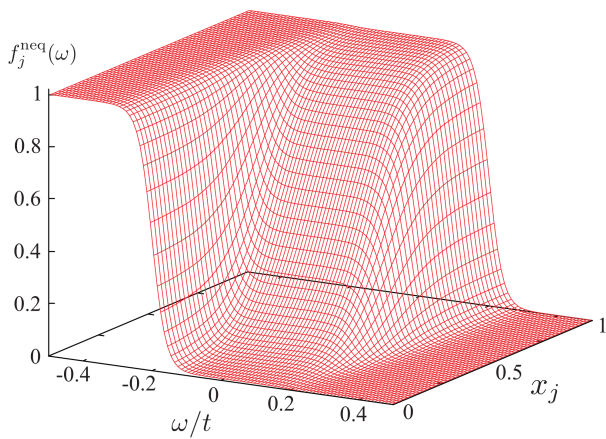


FIG. 6. The nonequilibrium distribution function $f_j^{\text{neq}}(\omega)$ approximated by Eq. (46) for $\gamma_{\text{imp}}/t = \sqrt{0.05}$. The exact distribution is shown in Fig. 3(b).

and right reservoirs at each energy ω , which can be expressed as

$$f_j^{\text{neq}}(\omega) = [1 - x_j]f(\omega - \mu_L) + x_j f(\omega - \mu_R). \quad (49)$$

This nonequilibrium distribution function is obtained by solving the transport equation (2) in the absence of elastic scattering [31, 40],

$$D\partial_x^2 f_x^{\text{neq}}(\omega) = 0, \quad (50)$$

under the boundary conditions in Eqs. (3) and (4). Thus, Figs. 3(a)-(c) demonstrate that the distribution functions in the ballistic-diffusive crossover regime are well described within our framework.

Figure 7(a) shows the electrostatic potential φ_j along the wire in the ballistic-diffusive crossover regime. In the ballistic limit ($\gamma_{\text{imp}} = 0$), the voltage drops at the contacts ($x_j = 0$ and $x_j = 1$) between the wire and the reservoirs, while the potential φ_j is constant in the bulk of the wire [88–91]. In this case, the resistance is located at the contacts, whereas no dissipation occurs in the bulk of the wire. This resistance of the ballistic wire is known as the contact resistance [89, 92]. On the other hand, as the impurity scattering strength γ_{imp} increases, the potential φ_j profile changes from the flat profile with large jumps at the contacts to a smooth linear profile connecting the electrochemical potentials $\mu_{\alpha=L,R}$ in the reservoirs. In this case, dissipation occurs throughout the wire, resulting in diffusive Ohmic transport. We note that the crossover from ballistic to Ohmic transport can also be directly observed through electron transport properties, as discussed in Appendix B.

To summarize, in the presence of elastic scattering from impurities, the distribution function $f_j^{\text{neq}}(\omega)$ depends on position x_j while maintaining its characteristic two-step structure in the low-temperature regime ($T_{\text{env}} \ll \mu_L - \mu_R$). Thus, when the wire length is shorter than the electron inelastic mean free path and inelastic

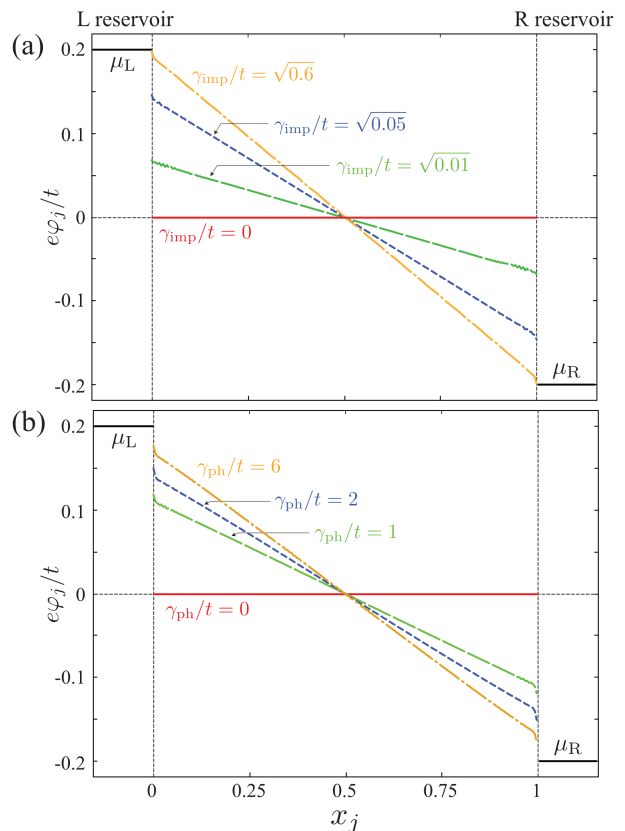


FIG. 7. Profile of the electrostatic potential φ_j for different values of (a) impurity scattering strength γ_{imp} and (b) electron-phonon coupling strength γ_{ph} . The electrochemical potential in the α reservoir is fixed at $\mu_{\alpha}/t = \pm 0.2$. In panel (a), we set $\gamma_{\text{ph}} = 0$, while in panel (b), we set $\gamma_{\text{imp}} = 0$.

scattering is negligible, the local equilibrium assumption is no longer valid so that effective temperature T_{eff} and chemical potential μ_{eff} cannot be defined in the entire ballistic-diffusive crossover regime.

B. Crossover from the non-equilibrium to the local-equilibrium regime

We next discuss how inelastic scattering from phonons affects the form of the distribution function. As shown in Figs. 3(a), (d), and (g), the distribution function depends on position x_j due to inelastic scattering from phonons. Moreover, Fig. 7(b) shows that the profile of the electrostatic potentials φ_j changes from the flat profile to the linear profile connecting the electrochemical potentials μ_{α} in the reservoirs, with increasing the electron-phonon coupling strength γ_{ph} . These behaviors are similar to those observed when increasing the impurity scattering strength γ_{imp} , as discussed in Sec. III A.

In addition to this effect, inelastic scattering from phonons smears out the characteristic two-step structure in the nonequilibrium distribution function. Figure 8

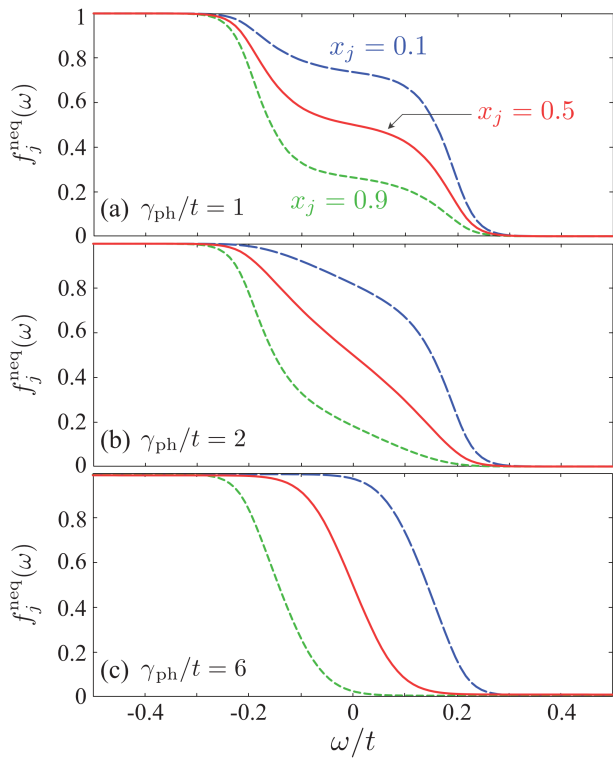


FIG. 8. Calculated distribution function $f_j^{\text{neq}}(\omega)$ for (a) $\gamma_{\text{ph}}/t = 1$, (b) $\gamma_{\text{ph}}/t = 2$, and (c) $\gamma_{\text{ph}}/t = 6$. We set $\gamma_{\text{imp}} = 0$ for all panels.

shows the distribution function at $x_j = 0.1, 0.5$, and 0.9 for different electron-phonon coupling strengths γ_{ph} . As the electron-phonon coupling increases, the nonequilibrium distribution function having the two-step structure gradually evolves into a Fermi-Dirac-like distribution function. We see from Fig. 8(c) that in the presence of strong inelastic scattering from phonons, the distribution function $f_j^{\text{neq}}(\omega)$ can be well approximated by the Fermi-Dirac distribution function,

$$f_j^{\text{neq}}(\omega) \simeq \frac{1}{e^{(\omega - e\varphi_j)/T_{\text{env}}} + 1}, \quad (51)$$

even in the presence of bias voltage. In this regime, the electrons reach local equilibrium through inelastic scattering from phonons, which redistributes the electron distribution distorted by the bias voltage [31, 70]. Since the distribution function can be well fitted by the Fermi-Dirac distribution function, the effective temperature and chemical potential are physically meaningful quantities, corresponding to the phonon temperature T_{env} and the electrostatic potential $e\varphi_j$, respectively.

We note that while electron-phonon interactions are the dominant source of inelastic scattering typically above 1K, electron-electron interactions become the leading inelastic process at lower temperatures [70, 73–75]. Electron-electron scattering smears out the two-step structure in the distribution function induced by the bias voltage, as does electron-phonon scattering. In particu-

lar, when the wire length is sufficiently long compared to the electron-electron mean free path, electrons reach local equilibrium through electron-electron scattering [31, 34–36, 70]. In this state, commonly referred to as the “hot-electron state”, the distribution function $f_j^{\text{neq}}(\omega)$ can be well approximated by the Fermi-Dirac distribution function characterized by position-dependent temperature T_j^{eff} and electrochemical potential μ_j^{eff} , given by [31, 34–36, 70]

$$f_j^{\text{neq}}(\omega) \simeq \frac{1}{e^{(\omega - \mu_j^{\text{eff}})/T_j^{\text{eff}}} + 1}. \quad (52)$$

As mentioned in Sec. II A, addressing the effects of electron-electron interactions on the distribution function lies beyond the scope of this work. Incorporating these correlation effects into our scheme and investigating the distribution function in the hot-electron regime remains an important challenge.

IV. SUMMARY

In summary, we have developed a theoretical framework to describe the nonequilibrium distribution function in a quasi-one-dimensional metal wire connected between two electrodes with different electrochemical potentials. The voltage-biased wire was modeled as a tight-binding chain connected to equilibrium reservoirs with different electrochemical potentials at both ends. We calculated the nonequilibrium distribution function in the wire using the nonequilibrium Green’s function technique. For electron scattering processes in the wire, we considered both elastic scattering from impurities and inelastic scattering from phonons within the self-consistent Born approximation.

We have demonstrated that the nonequilibrium distribution functions in various regimes are well described within our framework. In the ballistic regime, where electron scattering in the wire is negligible, the distribution function is spatially uniform and is given by the simple average of the Fermi-Dirac distribution functions in both reservoirs. In the diffusive regime dominated by elastic scattering from impurities, the distribution function linearly interpolates between the Fermi-Dirac distribution functions in the reservoirs at every energy level. Moreover, in the local equilibrium regime with strong electron-phonon scattering, electrons thermalize with phonons, and the distribution function can be well approximated by the Fermi-Dirac distribution function characterized by the phonon temperature and the local electrostatic potential.

We have also calculated the electrostatic potential along the metal wire. In the ballistic regime, the potential is constant along the wire and the voltage drops only at the contacts between the wire and the reservoirs. On the other hand, when electron-impurity or electron-phonon scattering is present, the voltage drops in the

bulk of the wire, resulting in a linear profile connecting the electrochemical potentials in both reservoirs.

We end by noting that our scheme can be readily extended to other nonequilibrium systems. For example, by combining with the Nambu Green's function technique [93], our scheme can be applied to superconducting heterostructures, such as a voltage-biased normal-metal wire between superconducting electrodes [94] and a voltage-biased superconducting wire between normal-metal electrodes [95–103]. It can also be applied to periodically driven systems, such as a metal wire under ac voltage [104, 105] and electron gases exposed to time-periodic electric field [106, 107], by combining with the Floquet Green's function technique [108]. In these systems, nonequilibrium distribution functions having characteristic structures can give rise to a variety of exotic quantum many-body phenomena that have not been observed in systems in (local) equilibrium. Exploring such nonequilibrium phenomena is currently one of the most exciting challenges in condensed matter physics, and our scheme would contribute to the further development of this research field.

ACKNOWLEDGMENTS

We gratefully thank H. Pothier for useful comments and for drawing our attention to relevant references. We also thank K. Yoshimi, S. Sumita, and Y. Ohashi for stimulating discussions. T.K. was supported by MEXT and JSPS KAKENHI Grant-in-Aid for JSPS fellows Grant No. JP24KJ0055. Y.K. was supported by JSPS KAKENHI No. JP21H01032. This research was also supported by Joint Research by the Institute for Molecular Science (IMS program No. 23IMS1101) (Y.K.) Some of the computations in this work were done using the facilities of the Supercomputer Center, the Institute for Solid State Physics, the University of Tokyo.

Appendix A: Numerical implementation

1. Numerical Hilbert transformation

To efficiently evaluate $\Sigma_{\text{ph}}^{\mathcal{R}}(\omega)$ in Eq. (32a), we take advantage of the fact that the imaginary part $\text{Im}\Sigma_{\text{ph}}^{\mathcal{R}}(\omega)$ of the self-energy is obtained from the lesser and the greater components $\Sigma_{\text{ph}}^{\lessgtr}(\omega)$ in Eq. (35) as [63]

$$\text{Im}\Sigma_{\text{ph}}^{\mathcal{R}}(\omega) = \frac{1}{2i} [\Sigma_{\text{ph}}^{\lessgtr}(\omega) - \Sigma_{\text{ph}}^{\lessgtr}(\omega)]. \quad (\text{A1})$$

The real part is then evaluated from the Kramers-Kronig relation, given by

$$\text{Re}\Sigma_{\text{ph}}^{\mathcal{R}}(\omega) = \frac{1}{\pi} \mathcal{P} \int_{-\infty}^{\infty} d\omega' \frac{\text{Im}\Sigma_{\text{ph}}^{\mathcal{R}}(\omega')}{\omega' - \omega}. \quad (\text{A2})$$

Here, \mathcal{P} denotes the Cauchy principal value integral.

The direct computation of the Hilbert transformation in Eq. (A2) is typically a numerically demanding task. To circumvent this difficulty, we employ the interpolation technique developed in Refs. [109, 110]: We approximate the function $\text{Im}\Sigma_{\text{ph}}^{\mathcal{R}}(\omega)$ by a linear interpolation to the values $\text{Im}\Sigma_{\text{ph}}^{\mathcal{R}}(\omega_j)$ known at discrete grid points $\{\omega_j\}$, expressed as

$$\text{Im}\Sigma_{\text{ph}}^{\mathcal{R}}(\omega) \simeq \sum_j \text{Im}\Sigma_{\text{ph}}^{\mathcal{R}}(\omega_j) \Phi_j(\omega). \quad (\text{A3})$$

Here, $\Phi_j(\omega)$ is the kernel function associated with the linear interpolation, given by

$$\begin{aligned} \Phi_j(\omega) &= \frac{\omega - \omega_{j-1}}{\omega_j - \omega_{j-1}} [\Theta(\omega_j - \omega) - \Theta(\omega_{j-1} - \omega)] \\ &+ \frac{\omega_{j+1} - \omega}{\omega_{j+1} - \omega_j} [\Theta(\omega_{j+1} - \omega) - \Theta(\omega_j - \omega)]. \end{aligned} \quad (\text{A4})$$

Substituting the approximated $\text{Im}\Sigma_{\text{ph}}^{\mathcal{R}}(\omega)$ into Eq. (A2), we have

$$\text{Re}\Sigma_{\text{ph}}^{\mathcal{R}}(\omega) = \sum_j \text{Im}\Sigma_{\text{ph}}^{\mathcal{R}}(\omega_j) \phi_j(\omega). \quad (\text{A5})$$

Here,

$$\begin{aligned} \phi_j(\omega) &= \frac{1}{\pi} \mathcal{P} \int_{-\infty}^{\infty} d\omega' \frac{\Phi_j(\omega')}{\omega' - \omega} \\ &= \frac{1}{\pi} \left[\frac{\omega - \omega_{j-1}}{\omega_j - \omega_{j-1}} \log \left| \frac{\omega_{j-1} - \omega}{\omega_j - \omega} \right| \right. \\ &\quad \left. + \frac{\omega - \omega_{j+1}}{\omega_j - \omega_{j+1}} \log \left| \frac{\omega - \omega_j}{\omega - \omega_{j+1}} \right| \right] \end{aligned} \quad (\text{A6})$$

is the transformation kernel [109, 110]. With this kernel, the Hilbert transformation in Eq. (A2) can be performed by the simple summation in Eq. (A5).

2. Inverse of a tridiagonal matrix

As shown in Ref. [111], the inverse of a non-singular tridiagonal matrix

$$\mathbf{T} = \begin{pmatrix} a_1 & b_1 & & & \\ c_1 & a_2 & b_2 & & \\ & \ddots & \ddots & \ddots & \\ & & c_{n-2} & a_{n-1} & b_{n-1} \\ & & & c_{n-1} & a_n \end{pmatrix} \quad (\text{A7})$$

is given by

$$(T^{-1})_{ij} = \begin{cases} (-1)^{i+j} b_i \cdots b_{j-1} \theta_{i-1} \phi_{j+1} / \theta_n & (i < j) \\ \theta_{i-1} \phi_{j+1} / \theta_n & (i = j) \\ (-1)^{i+j} c_j \cdots c_{i-1} \theta_{j-1} \phi_{i+1} / \theta_n & (i > j) \end{cases}, \quad (\text{A8})$$

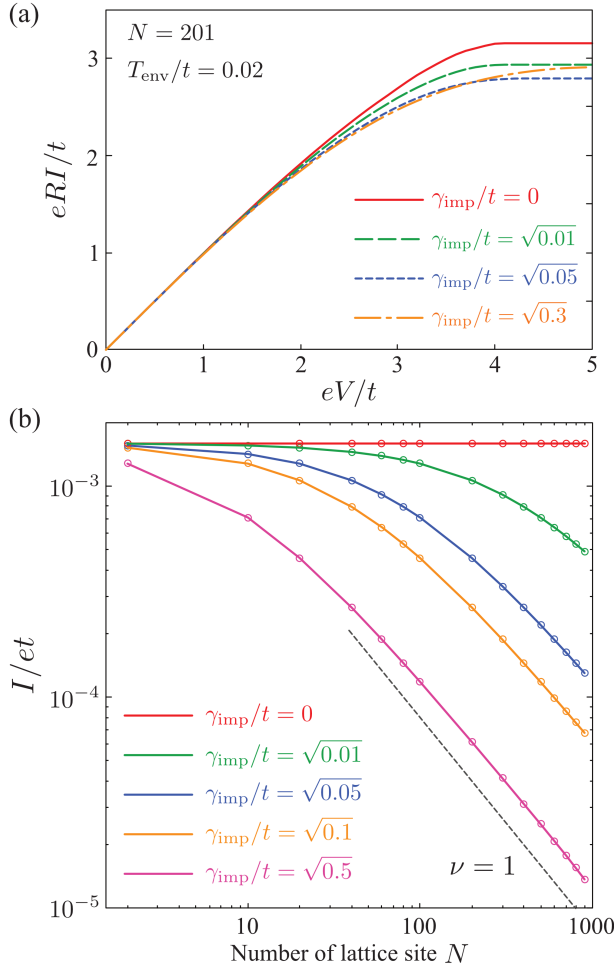


FIG. 9. (a) Voltage-current characteristics of the metal wire and (b) system size (number of lattice site N) dependence of the current through the wire. We show the results for different values of impurity scattering strength γ_{imp} . In panel (a), the current is normalized with the linear resistance R . In panel (b), the bias voltage is set to $eV/t = 0.01$.

where θ_i satisfies the recurrence relation

$$\theta_i = a_i \theta_{i-1} - b_{i-1} c_{i-1} \theta_{i-2} \quad (2 \leq i \leq n) \quad (\text{A9})$$

with initial conditions $\theta_0 = 1$, $\theta_1 = a_1$. For ϕ_j , we have

$$\phi_i = a_i \phi_{i+1} - b_i c_i \phi_{i+2} \quad (n-1 \geq i \geq 1) \quad (\text{A10})$$

with initial conditions $\phi_{n+1} = 1$ and $\phi_n = a_n$.

Appendix B: Electron transport properties of the metal wire in the ballistic-diffusive crossover regime

The charge current $I_{\alpha=L,R}(t)$ from the α reservoir to the wire is determined from the rate of change in the

number of electrons in the α reservoirs [65, 112, 113]:

$$\begin{aligned} I_\alpha(t) &= -e \frac{d}{dt} \sum_{\mathbf{k}} \langle a_{\alpha,\mathbf{k}}^\dagger(t) a_{\alpha,\mathbf{k}}(t) \rangle \\ &= -2e \text{Re} \sum_{\mathbf{k}} \left[t_{\text{lead}} G_{\text{mix},\alpha,\mathbf{k}}^<(t,t) \right]. \end{aligned} \quad (\text{B1})$$

Here, we have introduced the mixed lesser function $G_{\text{mix},\alpha,\mathbf{k}}^<(t,t')$, defined by

$$G_{\text{mix},\alpha,\mathbf{k}}^<(t,t') = i \langle a_{\mathbf{k}}^\dagger(t') c_{i_\alpha}(t) \rangle, \quad (\text{B2})$$

where $i_\alpha = 1$ if $\alpha = L$ and $i_\alpha = N$ if $\alpha = R$. When the system is in a NESS, this function is evaluated as [65, 112, 113]

$$\begin{aligned} G_{\text{mix},\alpha,\mathbf{k}}^<(t,t) &= -t_{\text{lead}}^* \int_{-\infty}^{\infty} d\omega \left[G_{i_\alpha i_\alpha}^{\mathcal{R}}(\omega) \mathcal{G}_{\alpha,\mathbf{k}}^<(\omega) \right. \\ &\quad \left. + G_{i_\alpha i_\alpha}^<(\omega) \mathcal{G}_{\alpha,\mathbf{k}}^{\mathcal{A}}(\omega) \right]. \end{aligned} \quad (\text{B3})$$

Here, $G_{i_\alpha i_\alpha}^{\mathcal{R},<}(\omega)$ is the dressed Green's function, obtained from the Dyson equations (18) and (19), while $\mathcal{G}_{\alpha,\mathbf{k}}^{\mathcal{A},<}(\omega)$ represents the noninteracting Green's function in the α reservoir, given in Eqs. (23a) and (23b). Substituting Eq. (B3) into Eq. (B1) and performing the \mathbf{k} summation, we obtain the charge current as

$$\begin{aligned} I_\alpha &= 2e \text{Re} \int_{-\infty}^{\infty} \frac{d\omega}{2\pi} \left[G_{i_\alpha i_\alpha}^{\mathcal{R}}(\omega) \Sigma_{\text{lead},\alpha}^<(\omega) \right. \\ &\quad \left. + G_{i_\alpha i_\alpha}^<(\omega) \Sigma_{\text{lead},\alpha}^{\mathcal{A}}(\omega) \right] \\ &= 2e \text{Re} \int_{-\infty}^{\infty} \frac{d\omega}{2\pi} \text{Tr} \left[\mathbf{G}^{\mathcal{R}}(\omega) \Sigma_{\text{lead},\alpha}^<(\omega) \right. \\ &\quad \left. + \mathbf{G}^<(\omega) \Sigma_{\text{lead},\alpha}^{\mathcal{A}}(\omega) \right] \\ &= 2ie \int_{-\infty}^{\infty} \frac{d\omega}{2\pi} \text{Tr} \left[\mathbf{\Gamma}_\alpha \left[f(\omega - \mu_\alpha) \left[\mathbf{G}^{\mathcal{R}}(\omega) - \mathbf{G}^{\mathcal{A}}(\omega) \right] \right. \right. \\ &\quad \left. \left. + \mathbf{G}^<(\omega) \right] \right]. \end{aligned} \quad (\text{B4})$$

In deriving the third line, we have used Eqs. (24a) and (24b). Noting that $I = I_L = -I_R$ in the NESS, we obtain a symmetric expression for the current, known as the Meir-Wingreen formula [112], as

$$\begin{aligned} I &= ie \int_{-\infty}^{\infty} \frac{d\omega}{2\pi} \text{Tr} \left[\left[\mathbf{\Gamma}_L f(\omega - \mu_L) - \mathbf{\Gamma}_R f(\omega - \mu_R) \right] \right. \\ &\quad \left. \times \left[\mathbf{G}^{\mathcal{R}}(\omega) - \mathbf{G}^{\mathcal{A}}(\omega) \right] + \left[\mathbf{\Gamma}_L - \mathbf{\Gamma}_R \right] \mathbf{G}^<(\omega) \right]. \end{aligned} \quad (\text{B5})$$

We note that in the ballistic limit ($\gamma_{\text{imp}} = \gamma_{\text{ph}} = 0$), Eq. (B5) can be simplified by using Eq. (44), leading to

$$I = e \int_{-\infty}^{\infty} d\omega \left[f(\omega - \mu_L) - f(\omega - \mu_R) \right] T(\omega). \quad (\text{B6})$$

Here,

$$T(\omega) = \frac{2\gamma_{\text{lead}}^2}{\pi} |G_{1N}^{\mathcal{R}}(\omega)|^2 \quad (\text{B7})$$

represents the transmission probability of the ballistic wire. Equation (B6) is known as the Landauer formula [114, 115]. We emphasize that Eq. (B6) is valid only in the ballistic limit.

Figure 9(a) presents the voltage-current characteristics of the metal wire, computed from Eq. (B5). This result indicates that the bias voltage $eV/t = 0.4$, used in Fig. 3, lies in the linear transport regime ($I \propto V$) in the entire ballistic-diffusive crossover regime. We note that the current I saturates when the applied bias voltage V exceeds the bandwidth $W = 4t$ of the wire.

In the linear transport regime, the current I follows a power-law scaling with the system size (number of lattice

sites N) [89, 116]:

$$I \sim \frac{1}{N^\nu}. \quad (\text{B8})$$

As shown in Fig. 9(b), the current remains independent of the system size ($\nu = 0$) in the ballistic limit ($\gamma_{\text{imp}} = 0$). In contrast, in the presence of impurity scattering ($\gamma_{\text{imp}} \neq 0$), the current depends on the system size N . In particular, for $\gamma_{\text{imp}}/t = \sqrt{0.5}$, the current is inversely proportional to the system size ($\nu = 1$), which is a characteristic feature of an Ohmic conductor. These changes in the ballistic-diffusive crossover regime are consistent with results from the dephasing model [116–119] and self-consistent reservoir model [120, 121], both of which are widely used to study electron transport in the ballistic-diffusive crossover regime.

-
- [1] N. Goldman and J. Dalibard, Phys. Rev. X **4**, 031027 (2014).
- [2] M. Bukov, L. D’Alessio, and A. Polkovnikov, Adv. Phys. **64**, 139 (2015).
- [3] A. Eckardt and E. Anisimovas, New J. Phys. **17**, 093039 (2015).
- [4] T. Oka and S. Kitamura, Annu. Rev. Condens. Matter Phys. **10**, 387 (2019).
- [5] S. Yin, E. Galiffi, and A. Alù, eLight **2**, 8 (2022).
- [6] F. Harper, R. Roy, M. S. Rudner, and S. Sondhi, Annu. Rev. Condens. Matter Phys. **11**, 345 (2020).
- [7] T. Oka and H. Aoki, Phys. Rev. B **79**, 081406 (2009).
- [8] T. Kitagawa, E. Berg, M. Rudner, and E. Demler, Phys. Rev. B **82**, 235114 (2010).
- [9] N. H. Lindner, G. Refael, and V. Galitski, Nat. Phys. **7**, 490 (2011).
- [10] M. Ezawa, Phys. Rev. Lett. **110**, 026603 (2013).
- [11] Y. T. Katan and D. Podolsky, Phys. Rev. Lett. **110**, 016802 (2013).
- [12] J. Cayssol, B. Dóra, F. Simon, and R. Moessner, Phys. Stat. Sol. (RRL) **7**, 101 (2013).
- [13] R. Roy and F. Harper, Phys. Rev. B **96**, 155118 (2017).
- [14] M. S. Rudner and N. H. Lindner, Nat. Rev. Phys. **2**, 229 (2020).
- [15] R. El-Ganainy, K. G. Makris, M. Khajavikhan, Z. H. Musslimani, S. Rotter, and D. N. Christodoulides, Nat. Phys. **14**, 11 (2018).
- [16] K. Yamamoto, M. Nakagawa, K. Adachi, K. Takasan, M. Ueda, and N. Kawakami, Phys. Rev. Lett. **123**, 123601 (2019).
- [17] R. Hanai, A. Edelman, Y. Ohashi, and P. B. Littlewood, Phys. Rev. Lett. **122**, 185301 (2019).
- [18] R. Hanai and P. B. Littlewood, Phys. Rev. Res. **2**, 033018 (2020).
- [19] M. Fruchart, R. Hanai, P. B. Littlewood, and V. Vitelli, Nature **592**, 363 (2021).
- [20] H. Shen, B. Zhen, and L. Fu, Phys. Rev. Lett. **120**, 146402 (2018).
- [21] Z. Gong, Y. Ashida, K. Kawabata, K. Takasan, S. Higashikawa, and M. Ueda, Phys. Rev. X **8**, 031079 (2018).
- [22] K. Kawabata, K. Shiozaki, M. Ueda, and M. Sato, Phys. Rev. X **9**, 041015 (2019).
- [23] Y. Ashida, Z. Gong, and M. Ueda, Adv. Phys. **69**, 249 (2020).
- [24] D. S. Borgnia, A. J. Kruchkov, and R.-J. Slager, Phys. Rev. Lett. **124**, 056802 (2020).
- [25] E. J. Bergholtz, J. C. Budich, and F. K. Kunst, Rev. Mod. Phys. **93**, 015005 (2021).
- [26] N. Okuma and M. Sato, Annu. Rev. Condens. Matter Phys. **14**, 83 (2023).
- [27] H. Wu and J.-H. An, Phys. Rev. B **102**, 041119 (2020).
- [28] J. Casas-Vázquez and D. Jou, Phys. Rev. E **49**, 1040 (1994).
- [29] J. Casas-Vázquez and D. Jou, Rep. Prog. Phys. **66**, 1937 (2003).
- [30] H. Pothier, S. Guéron, N. O. Birge, D. Esteve, and M. H. Devoret, Phys. Rev. Lett. **79**, 3490 (1997).
- [31] S. Gueron, *Quasiparticles in a diffusive conductor: Interaction and pairing*, Theses, Université Pierre et Marie Curie - Paris VI (1997).
- [32] A. Anthore, F. Pierre, H. Pothier, and D. Esteve, Phys. Rev. Lett. **90**, 076806 (2003).
- [33] B. Huard, A. Anthore, N. O. Birge, H. Pothier, and D. Esteve, Phys. Rev. Lett. **95**, 036802 (2005).
- [34] B. Huard, *Interactions between electrons, mesoscopic Josephson effect and asymmetric current fluctuations*, Theses, Université Pierre et Marie Curie - Paris VI (2006).
- [35] F. Pierre, *Interaction électron-électron dans les fils mésoscopiques*, Theses, Université Pierre et Marie Curie - Paris VI (2000).
- [36] A. Anthore, *Mécanismes de décohérence dans les conducteurs mésoscopiques / Decoherence mechanisms in mesoscopic conductors*, Theses, Université Pierre et Marie Curie - Paris VI (2003).
- [37] E. S. Tikhonov, A. O. Denisov, S. U. Piatrusha, I. N. Khrapach, J. P. Pekola, B. Karimi, R. N. Jabdaraghi, and V. S. Khrapai, Phys. Rev. B **102**, 085417 (2020).
- [38] S. De Franceschi, R. Hanson, W. G. van der Wiel, J. M.

- Elzerman, J. J. Wijkema, T. Fujisawa, S. Tarucha, and L. P. Kouwenhoven, *Phys. Rev. Lett.* **89**, 156801 (2002).
- [39] Y.-F. Chen, T. Dirks, G. Al-Zoubi, N. O. Birge, and N. Mason, *Phys. Rev. Lett.* **102**, 036804 (2009).
- [40] N. T. Bronn, *Spectroscopy of correlated nanowires* (University of Illinois at Urbana-Champaign, 2013).
- [41] N. Bronn and N. Mason, *Phys. Rev. B* **88**, 161409 (2013).
- [42] M. Lebrat, P. Grišins, D. Husmann, S. Häusler, L. Corman, T. Giamarchi, J.-P. Brantut, and T. Esslinger, *Phys. Rev. X* **8**, 011053 (2018).
- [43] J. Mohan, *Universal particle and entropy transport in strongly interacting Fermi gases far from equilibrium*, Ph.D. thesis, ETH Zurich (2024).
- [44] J. Baselmans, A. Morpurgo, B. Van Wees, and T. Klapwijk, *Nature* **397**, 43 (1999).
- [45] R. Shaikhaidarov, A. F. Volkov, H. Takayanagi, V. T. Petrashov, and P. Delsing, *Phys. Rev. B* **62**, R14649 (2000).
- [46] J. J. A. Baselmans, B. J. van Wees, and T. M. Klapwijk, *Phys. Rev. B* **63**, 094504 (2001).
- [47] J. J. A. Baselmans, T. T. Heikkilä, B. J. van Wees, and T. M. Klapwijk, *Phys. Rev. Lett.* **89**, 207002 (2002).
- [48] J. Huang, F. Pierre, T. T. Heikkilä, F. K. Wilhelm, and N. O. Birge, *Phys. Rev. B* **66**, 020507 (2002).
- [49] P. Pandey, D. Beckmann, and R. Danneau, *Phys. Rev. B* **106**, 214503 (2022).
- [50] D. A. Abanin and L. S. Levitov, *Phys. Rev. Lett.* **94**, 186803 (2005).
- [51] T. Kawamura, R. Hanai, D. Kagamihara, D. Inotani, and Y. Ohashi, *Phys. Rev. A* **101**, 013602 (2020).
- [52] T. Kawamura, R. Hanai, and Y. Ohashi, *Phys. Rev. A* **106**, 013311 (2022).
- [53] T. Kawamura, Y. Ohashi, and H. T. C. Stoof, *Phys. Rev. B* **109**, 104502 (2024).
- [54] T. Kawamura and Y. Ohashi, *AAPPS Bulletin* **34**, 31 (2024).
- [55] I. A. Dmitriev, A. D. Mirlin, and D. G. Polyakov, *Phys. Rev. Lett.* **91**, 226802 (2003).
- [56] I. A. Dmitriev, M. G. Vavilov, I. L. Aleiner, A. D. Mirlin, and D. G. Polyakov, *Phys. Rev. B* **71**, 115316 (2005).
- [57] S. I. Dorozhkin, J. H. Smet, V. Umansky, and K. von Klitzing, *Phys. Rev. B* **71**, 201306 (2005).
- [58] S. I. Dorozhkin, A. A. Kapustin, V. Umansky, K. von Klitzing, and J. H. Smet, *Phys. Rev. Lett.* **117**, 176801 (2016).
- [59] J. Clarke, *Phys. Rev. Lett.* **28**, 1363 (1972).
- [60] M. Tinkham and J. Clarke, *Phys. Rev. Lett.* **28**, 1366 (1972).
- [61] M. Tinkham, *Phys. Rev. B* **6**, 1747 (1972).
- [62] A. Schmid and G. Schön, *Journal of Low Temperature Physics* **20**, 207 (1975).
- [63] J. Rammer, *Quantum Field Theory of Non-equilibrium States* (Cambridge University Press, 2007).
- [64] G. Stefanucci and R. van Leeuwen, *Nonequilibrium Many-Body Theory of Quantum Systems: A Modern Introduction* (Cambridge University Press, 2013).
- [65] H. Haug, A.-P. Jauho, *et al.*, *Quantum kinetics in transport and optics of semiconductors*, Vol. 2 (Springer, 2008).
- [66] K. Nagaev, *Physics Letters A* **169**, 103 (1992).
- [67] K. E. Nagaev, *Phys. Rev. B* **52**, 4740 (1995).
- [68] V. I. Kozub and A. M. Rudin, *Phys. Rev. B* **52**, 7853 (1995).
- [69] Y. Naveh, D. V. Averin, and K. K. Likharev, *Phys. Rev. B* **58**, 15371 (1998).
- [70] T. T. Heikkilä, *The physics of nanoelectronics: transport and fluctuation phenomena at low temperatures*, Vol. 21 (Oxford University Press, USA, 2013).
- [71] T. Holstein, *Ann. Phys.* **8**, 325 (1959).
- [72] T. Holstein, *Ann. Phys.* **8**, 343 (1959).
- [73] B. L. Altshuler, A. G. Aronov, and D. E. Khmel'nitsky, *Journal of Physics C: Solid State Physics* **15**, 7367 (1982).
- [74] A. L. Efros and M. Pollak, *Electron-electron interactions in disordered systems* (Elsevier, 2012).
- [75] F. Pierre, A. B. Gougam, A. Anthore, H. Pothier, D. Esteve, and N. O. Birge, *Phys. Rev. B* **68**, 085413 (2003).
- [76] A. Kaminski and L. I. Glazman, *Phys. Rev. Lett.* **86**, 2400 (2001).
- [77] G. Göppert, Y. M. Galperin, B. L. Altshuler, and H. Grabert, *Phys. Rev. B* **66**, 195328 (2002).
- [78] A. Cresti and G. P. Parravicini, *Phys. Rev. B* **78**, 115313 (2008).
- [79] P. W. Anderson, *Phys. Rev.* **109**, 1492 (1958).
- [80] This assumption is well justified when the metal wire lies on a substrate. In such cases, the phonons in the wire strongly couple to those in the substrate, and electron-phonon coupling does not significantly disturb the phonon states in the wire [70].
- [81] P. Pulay, *Chem. Phys. Lett.* **73**, 393 (1980).
- [82] P. P. Pratapa and P. Suryanarayana, *Chem. Phys. Lett.* **635**, 69 (2015).
- [83] A. S. Banerjee, P. Suryanarayana, and J. E. Pask, *Chem. Phys. Lett.* **647**, 31 (2016).
- [84] H. Ness, *Phys. Rev. E* **88**, 022121 (2013).
- [85] H. Ness, *Phys. Rev. B* **89**, 045409 (2014).
- [86] C. G. Broyden, *Math. Comp.* **19**, 577 (1965).
- [87] C. G. Broyden, *Math. Comp.* **21**, 368 (1967).
- [88] E. Scheer and J. C. Cuevas, *Molecular electronics: an introduction to theory and experiment*, Vol. 15 (World Scientific, 2017).
- [89] T. Stegmann, *Quantum transport in nanostructures: From the effects of decoherence on localization to magnetotransport in two-dimensional electron systems*, Ph.D. thesis, Duisburg, Essen, Universität Duisburg-Essen, 2014.
- [90] Y. Imry, *Introduction to mesoscopic physics* (Oxford university press, 2002).
- [91] S. Datta, *Quantum Transport: Atom to Transistor* (Cambridge University Press, 2005).
- [92] S. Datta, *Electronic Transport in Mesoscopic Systems*, Cambridge Studies in Semiconductor Physics and Microelectronic Engineering (Cambridge University Press, 1995).
- [93] Y. Nambu, *Phys. Rev.* **117**, 648 (1960).
- [94] F. Pierre, A. Anthore, H. Pothier, C. Urbina, and D. Esteve, *Phys. Rev. Lett.* **86**, 1078 (2001).
- [95] R. S. Keizer, M. G. Flokstra, J. Aarts, and T. M. Klapwijk, *Phys. Rev. Lett.* **96**, 147002 (2006).
- [96] N. Vercruyssen, T. G. A. Verhagen, M. G. Flokstra, J. P. Pekola, and T. M. Klapwijk, *Phys. Rev. B* **85**, 224503 (2012).
- [97] K. M. Seja and T. Löfwander, *Phys. Rev. B* **104**, 104502 (2021).
- [98] F. Hübler, J. C. Lemyre, D. Beckmann, and

- H. v. Löhneysen, Phys. Rev. B **81**, 184524 (2010).
- [99] K. Y. Arutyunov, H.-P. Auraneva, and A. S. Vasenko, Phys. Rev. B **83**, 104509 (2011).
- [100] R. Yagi, Phys. Rev. B **73**, 134507 (2006).
- [101] Y. Takane, J. Phys. Soc. Jpn. **75**, 074711 (2006).
- [102] Y. Takane, J. Phys. Soc. Jpn. **76**, 043701 (2007).
- [103] Y. Takane, J. Phys. Soc. Jpn. **78**, 064704 (2009).
- [104] A. V. Shytov, Phys. Rev. B **71**, 085301 (2005).
- [105] J. Gabelli and B. Reulet, Phys. Rev. B **87**, 075403 (2013).
- [106] O. Matsyshyn, J. C. W. Song, I. S. Villadieago, and L.-k. Shi, Phys. Rev. B **107**, 195135 (2023).
- [107] L.-k. Shi, O. Matsyshyn, J. C. W. Song, and I. S. Villadieago, Phys. Rev. Lett. **132**, 146402 (2024).
- [108] H. Aoki, N. Tsuji, M. Eckstein, M. Kollar, T. Oka, and P. Werner, Rev. Mod. Phys. **86**, 779 (2014).
- [109] T. Frederiksen, M. Paulsson, M. Brandbyge, and A.-P. Jauho, Phys. Rev. B **75**, 205413 (2007).
- [110] J. A. Vaitkus, C. S. Ho, and J. H. Cole, Phys. Rev. B **106**, 115420 (2022).
- [111] R. A. Usmani, Linear Algebra Appl. **212**, 413 (1994).
- [112] Y. Meir and N. S. Wingreen, Phys. Rev. Lett. **68**, 2512 (1992).
- [113] A.-P. Jauho, N. S. Wingreen, and Y. Meir, Phys. Rev. B **50**, 5528 (1994).
- [114] R. Landauer, IBM J. Res. Dev. **1**, 223 (1957).
- [115] R. Landauer, Philos. Mag. **21**, 863 (1970).
- [116] T. Jin, J. a. S. Ferreira, M. Filippone, and T. Giamarchi, Phys. Rev. Res. **4**, 013109 (2022).
- [117] S. Datta, Phys. Rev. B **40**, 5830 (1989).
- [118] M. J. McLennan, Y. Lee, and S. Datta, Phys. Rev. B **43**, 13846 (1991).
- [119] R. Golizadeh-Mojarad and S. Datta, Phys. Rev. B **75**, 081301 (2007).
- [120] J. L. D'Amato and H. M. Pastawski, Phys. Rev. B **41**, 7411 (1990).
- [121] D. Roy and A. Dhar, Phys. Rev. B **75**, 195110 (2007).